Numerical investigation of the flow field around low rise buildings due to a downburst event using Large Eddy Simulation.

Matthew Haines [a], Ian Taylor [a,b*1]

[a] *Department of Mechanical and Aerospace Engineering, University of Strathclyde, Glasgow, UK, G1 1XJ*
[b] *School of Engineering, James Watt Building South, University of Glasgow, Glasgow, G12 8QQ*

ABSTRACT : The transient lift and drag coefficients around a low rise cube of dimension $60mm$ and a portal building of dimensions $240 \times 130 \times 53mm$ with eaves height of $42mm$, which arise from the numerical simulation of an impinging jet or downburst are investigated. The numerical results were validated against a experimental results from a laboratory impinging jet simulator operating at the same scale. Having found the CFD simulation to match well with the laboratory scale the CFD was then used to visualise and interpret the flow field around the buildings. Common transient atmospheric boundary layer flow features, such as conical vortices, vortices on the rear face of a building, flow separation and vortex shedding were observed and could be used to explain the lift and drag results obtained. In particular, motion of the primary vortex from the downburst and its effect on the transient pressures on the building were identified, with strong pressure gradients observed for a number of configurations. Aspects of the flow phenomena were identified, which along with the strong pressure changes on the building surfaces, indicate areas of further research due to their potential impact on building and cladding design.

Keywords : Turbulent inlet, impinging jets, LES, downbursts, non-stationary analysis.

1. Introduction

In recent years, Wind Engineering researchers and practitioners have become increasingly interested the effects of extreme wind events, and particularly thunderstorm downbursts. During a downburst, an intense downward movement of air is formed by falling precipitation, buoyancy effects and intensified by other cloud processes such as the melting of ice and hail. This downwards moving column of air impinges on the ground, with the vortex ring being formed as the air

*Corresponding author
Email Address : Ian.Taylor@glasgow.ac.uk
[1]Based at University of Strathclyde prior to 20 July 2016 and at University of Glasgow from 20 July 2016.

is displaced radially outwards from the point of impingement. As the ring vortex translates along the ground away from the stagnation point, causing rapid changes in velocity, from which a very different flow field is produced, compared to those usually considered when assessing wind loads on structures (Sengupta and Sarkar, 2008; Zhang et al., 2013; Chay and Letchford, 2002b). Thunderstorm downbursts are therefore important from a wind engineering perspective as they are strongly non-stationary (Figure 1a), and also produce a different vertical velocity profile to the traditional "synoptic" winds characteristic of the logarithmic atmospheric boundary layer (ABL) profile (Figure 1b).

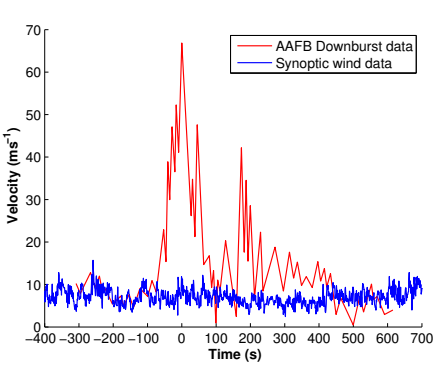

(a) Downburst velocity time history

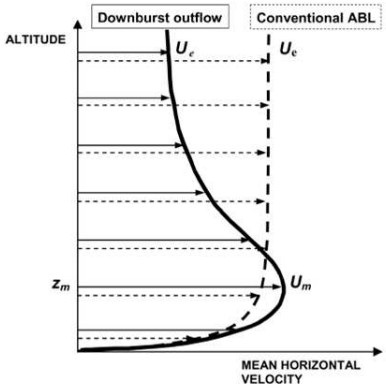

(b) Vertical velocity profile

Figure 1: a) Velocity time history comparison of a rural synoptic wind at $3m$ height (Sterling et al., 2006) and the Andrew's air force base (AAFB) downburst over rural terrain, $4.9m$ height, Fujita (1985); b) Schematic illustration of the mean streamwise velocity profile corresponding to a 'typical' downburst and a typical boundary layer or "synoptic" wind (Lin and Savory, 2006).

This difference to ABL flow complicates the investigation of pressure, drag and lift coefficients around buildings. The traditional ABL coefficients are usually normalised by the mean velocity of the wind field striking the building, but given the non-stationary nature of the downburst the idea of a mean velocity field is more problematic to define. There have been a number of approaches used including normalising the pressure coefficient time history by the 50 point running mean of the velocity time history on the roof face (Chay and Letchford, 2002b). Lombardo (2009) took a similar approach but normalised the velocity by a $3s$ mean instead of a 50 point moving average. However, regardless of the method used there are difficulties with direct comparison to existing ABL pressure coefficients because of the different methods that are required to calculate the coefficients for the two wind field types.

In order to investigate wind loading around buildings due to downburst flows, engineers generally have to resort to simulations (experimental or numerical) of the phenomenon, as they are difficult to forecast and cover only a small area. The most common of these is the impinging jet simulator, either constructed in

a laboratory, for example Holmes (1992) and Xu and Hangan (2008) or modelled numerically, for example (Selvam and Holmes, 1992) and Kim and Hangan (2007). These models can then be scaled to the limited full scale data (Jesson et al., 2015) and then model buildings placed in the flow with the resulting pressure fields analysed (although there are difficulties with selecting appropriate scaling for the simulations). While impinging jet models are not perfect they provide a simple way of analysing pressures around buildings without having to resort to time consuming full scale experiments and given the computational resources required to undertake numerical simulations of full scale data downburst events.

Lombardo (2009) examined the response of the Wind Engineering Research and Fluids Laboratory (WERFL) building a pressure tapped $9.14 \times 13.7 \times 4.0m$ cuboid, to full scale downburst winds. The peak pressure coefficients were compared to the building design codes given in ASCE (2006) and it was found that the peak pressures did not generally exceed the values in the code. However, in some instances there was a rapid increase in suction on the roof of the WERFL building which then exceeded the values given by ASCE (2006). It was hypothesised that when the downburst winds struck the edges of the building they were ideally suited to producing conical vortices which extended from the roof edges (Wu, 2001). However, it should be kept in mind that the choice of formula and gust duration greatly altered the number of events where design values were exceeded and differences in the formulae between the code and downburst pressure coefficients may make comparisons unreliable.

There have also been studies using impinging jet simulators to simulate downbursts, notably Chay and Letchford (2002b) who examined the pressure and drag coefficients around a cube in a translating impinging jet. Comparing these results with the ABL work of Castro and Robins (1977) revealed that the impinging jet flow did exceed the ABL flow pressure coefficients (1.5 compared to 0.9 on the windward face), but only briefly. On average the ABL coefficients were still higher over a similar time period. For the impinging jet the drag and lift coefficients also showed little difference to individual point pressure measurements, indicating that the flow was well correlated across the surface of the cube.

Sengupta and Sarkar (2008) also examined the flow around a cube, using a large eddy CFD simulation and laboratory based translating impinging jet simulator. The results from both simulations matched each other well and like Chay and Letchford (2002b) found to exceed ABL values with a maximum drag exceeded on the building front face (1.4) and maximum lift exceeded (-1.0) on the roof. However, neither of these studies attempted to visualise, or indeed hypothesise the causes of these pressures around the buildings.

Zhang et al. (2013) examined pressures around a portal building with two roof pitches (16° and 35°), at five distances from the centre of impingement ($\frac{r}{D} = 0.0$, $\frac{r}{D} = 0.5$, $\frac{r}{D} = 1.0$, $\frac{r}{D} = 1.5$ and $\frac{r}{D} = 2.0$) and three yaw angles (0°, 45° and 90°) and also used flow visualisation to try and identify the flow phenomena responsible for producing the pressures. In the simulated downburst winds the surface pressures on the portal buildings exceeded or matched those

defined for ABL winds by ASCE (2010), which would lead to greater wind loads. The maximum exceedance occurred at $\frac{r}{D} = 0.5$ when loadings were almost twice the pressures defined by ASCE (2010). The flow visualisation revealed that the causes of these exceedances varied depending on the yaw angle of the building. At the 45° yaw angle with the 16° roof pitch conical vortices were formed on the roof which increased the risk of damage to roof edges. However, at the 90° yaw angle low pressure bands were formed across the roof for both building pitches, formed by the flow separating at the windward / roof face edge.

Jubayer et al. (2016) investigated the wind loads on a low-rise building due to a laboratory simulated downburst, using the WindEEE Dome at Western University, Canada. A jet diameter of $3.2m$ was used with a generic low rise portal type building, scaled geometrically at $1:100$, corresponding to a full scale size of approximately $57m \times 37m \times 12m$. Pressure taps were included on the side faces and the roof, with readings taken for various building orientations. Varying loads on the roof, upward or downward, were found depending on building orientation and also corner vortices were identified at the eaves leading edges for some angles. Differences in magnitude between downburst and ABL pressures were also noted, again highlighting the necessity of considering non-synoptic type flows.

Jesson et al. (2015) further examined the pressures around a portal building with dimensions $240 \times 130 \times 53mm$, and with eaves height of $42mm$ at three yaw angles, 0°, 45° and 90° and also at different heights. A cube building at different heights was also examined so a comparison could be made to Chay and Letchford (2002b). Firstly it was found that there were stronger pressure gradients on the roof of the portal building than the cube building, especially at the 0° yaw angle where the cube distributions were relatively uniform across the roof face. Adjusting the yaw angle caused sharp gradients of pressure to form on both buildings, extending from the windward edge across the roof. These were assumed to be formed from conical vortices as they were in Zhang et al. (2013).

Unfortunately because of the location of the simulator within an open laboratory, Jesson et al. (2015) could not use the flow visualisation to confirm these hypotheses. Instead the data from the simulations of Jesson et al. (2015) were used to verify an LES simulation, the details, results and limitations of which are described in Haines et al. (2015).

This paper expands upon the work of Haines et al. (2015) using the numerical model developed to examine the pressure fields around two model buildings, a cube and portal building, with the same experimental setup and scale of Jesson et al. (2015). Firstly the simulation methodology is described, the results section then examines the match between between the CFD model and experimental data for the various building models, then discusses the potential causes of these pressures and finally compares them to ABL cases. Comparisons are also made to previous downburst studies throughout.

2. Simulation Methodology

The detailed experimental methodology of the CFD domain, along with details of mesh sensitivity investigations, can be found in Haines et al. (2015) and is briefly summarised here for convenience of the reader. A domain of $9.8 \times 9.8 \times 2.4m$ was used with $\approx 24 \times 10^6$ cells, depending on the building size used and is illustrated in Figure 2.

In Haines et al. (2015), various turbulence modelling schemes were assessed, and the standard OpenFOAM dynamic Smagorinsky LES turbulence model, which was found to be most suitable, is used for this investigation. The mesh density in the flow region of interest for the impinging jet was around $10mm$. The sides of the domain were treated as outlets and the boundary conditions were treated as von Neumann (zero gradient). The remaining domain boundaries were treated as walls with the pressure boundary condition being zero gradient and the velocity condition used the OpenFOAM wall function nutUWallFunction as the mesh was not fine enough to have a Y^+ value of 1. The peak velocity in the simulation ($\sim 20ms^{-1}$) gave a Y^+ value of ≈ 100 in the near building region, consistent with previous research (Sengupta and Sarkar (2008)).

Also visible in Figure 2 (in the upper centre of the domain) is a cylinder, with diameter of $1m$, the bottom face of which is $1.9m$ from the ground plane, which acts as the flow inlet. The inlet condition for the jet was a slightly modified version of the turbulent inlet of Kornev and Hassel (2007), which used a divergence free approach based on the digital filter method (often called the random spot method). However, this approach tended to produce unrealistic pressure fluctuations as the mass flux entering the computational domain was not equal to the mass flux expected from the mean field. To resolve this a mass flux correction term from Kim et al. (2013) and Poletto et al. (2013) was applied to the flow field across the inlet, to reduce the pressure fluctuations to slightly above the laboratory case. The inlet jet had a mean velocity of $13.4ms^{-1}$, with turbulence intensity of 17% and length scale of 0.11 (post-calculation), compared with respectively $13.4ms^{-1}$, 16% and 0.1 from the experiments (Jesson et al. (2015)).

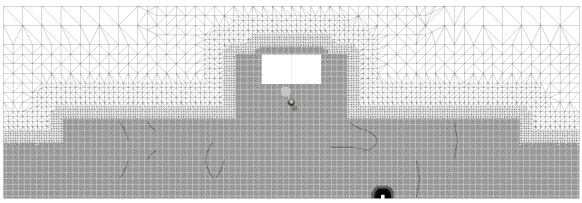

Figure 2: The numerical model domain and mesh.

Within the numerical domain a model building was also placed, with the dimensions of the cube or portal building used by Jesson et al. (2015), which had dimensions of $60 \times 60 \times 60mm$ and $240 \times 130 \times 53mm$ portal building

with eaves height of $42mm$ respectively. As highlighted in Jesson et al. (2015), based on the building dimension in the radial direction and the maximum radial velocity, this corresponds to a Reynolds number of $\sim 8 \times 10^4$. The mesh density near all of the buildings was $1.25mm$ and the mesh local to the cube and portal is illustrated in Figures 3a and 3b respectively. The boundary conditions used around the buildings were the same as the walls, zero gradient for pressure and a nutUWallFunction for velocity.

As highlighted, the dimensions in the simulation are matched to the experimental configuration, both for the building dimensions and also the $1m$ diameter impinging jet. As discussed in Sterling et al. (2011), scaling of the transient winds characteristic of downburst flows is not straightforward and is often open to interpretation. Additionally, data from full scale events is not plentiful, and has significant variations with downburst diameters ranging from $1km$ to $3km$ (Lin (2010)). Based on the estimated diameter of the Andrews air force base (AAFB) downburst (Fujita (1985)), it is felt that the length scale of the experimental facility is around $1 : 1600$ and a velocity scale in the range $1 : 2.5 - 1 : 3$ (Jesson et al. (2015)). The building dimensions were selected to provide the same ratio of cube side length to jet diameter as used in Chay and Letchford (2002a) for comparison purposes, and also to strike a balance with practicalities of having a model of sufficient size for incorporating instrumentation. However, the scaling of the experiments imply a small downdraft or a large building (Sterling et al. (2011)).

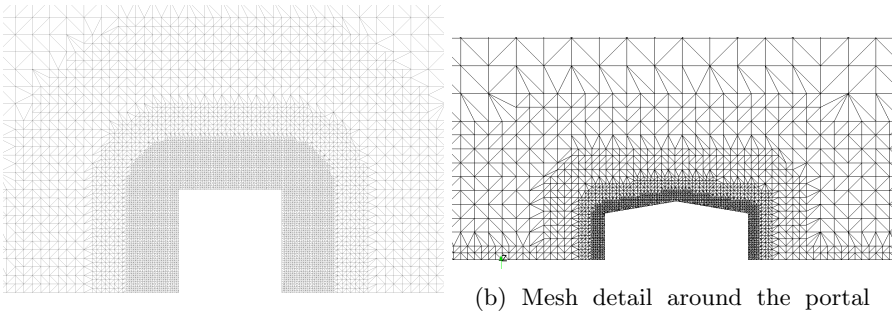

(a) Mesh detail around the cube building

(b) Mesh detail around the portal building

Figure 3: Numerical model domain and mesh with detail around a) the cube and b) the portal building

In order to match with the study of Jesson et al. (2015) each building had pressure taps placed as given by Figures 4a and 4b. The experiments recorded pressure measurements on the building surfaces for both buildings at three yaw angles, $0°$, $45°$ and $90°$. Additionally, the buildings could be recessed into the ground plane, to consider the structures at different heights. In this investigation, simulations are undertaken for the cube at two heights, $0mm$ (full height) and $40mm$, and at two yaw angles, $0°$ and $45°$. For the portal building, all three yaw angles are considered though only results for the full height are simu-

lated. Results for the lowest heights of the cube and lower heights of the portal building are not presented as the proximity of the measurement locations to the ground means the results are affected by interactions with the ground plane and do not add useful conclusions to the results discussed herein.

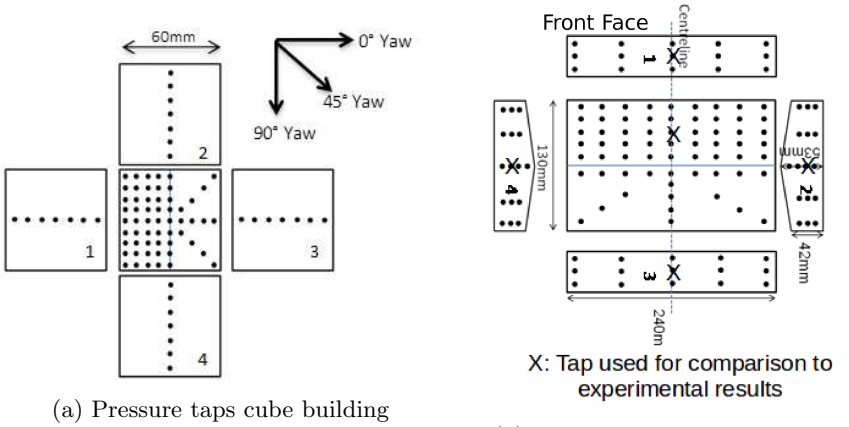

(a) Pressure taps cube building

(b) Pressure taps portal building

Figure 4: The location of the pressure taps on the study of Jesson et al. (2015) for a) the cube and b) the portal building.

The pressure coefficients (1) and drag coefficients (2) were calculated using the same formula and choice of variables as Jesson et al. (2015),

$$C_p = \frac{p - p_{ref}}{\frac{1}{2}\rho V^2} \tag{1}$$

$$C_d = \frac{1}{A_s}\int_{A_s} C_p dA \tag{2}$$

where C_p is the pressure coefficient, C_d is the drag coefficient, p is the measured pressure on the tap, p_{ref} a reference pressure, in this case atmospheric pressure as the buildings were sealed and V is the reference velocity. C_p is the pressure coefficient calculated for a tap from equation (1) and A_s is the area of the surface for which the force coefficient is being calculated, that is front face of building to radial drag, side face for lateral drag and roof for the lift. In this case the maximum velocity recorded in the laboratory (or numerical) simulation was $\approx 21ms^{-1}$, and this value was chosen for the normalisation because it is similar to the eaves height normalisation used for ABL flows. In an ABL flow the maximum velocity occurs at eaves height, whereas in a thunderstorm downburst this may not be the case mainly due to the different vertical velocity profile illustrated in Figure 1. This was also the normalisation velocity used by Jesson et al. (2015), so is consistent with the approach used in the experimental data to which the numerical results are being compared.

Three aerodynamic force components were determined from the numerical results, calculated to be consistent with those obtained by Jesson et al. (2015). These were the radial, lateral and lift components of aerodynamic force which are illustrated in Figure 5. Radial drag is defined as the force in the same direction as the primary vortex as it convects radially outwards from the impingement point on the surface (i.e. flow direction) and lateral drag is defined as the force perpendicular to the flow direction.

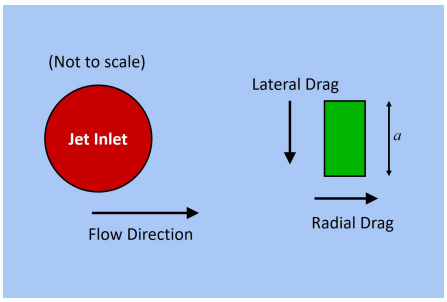

(a) Plan view

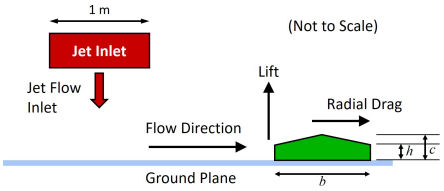

(b) Side view

Figure 5: The orientation of the radial, lateral and lift drag components in relation to the model buildings and experimental domain. Dimensions of portal building are $a = 240mm$, $b = 130mm$ and $c = 53mm$, with eaves at height, $h = 42mm$. Cube building has dimensions, $a = b = c = 60mm$.

3. Results and Discussion

3.1. Comparison of Aerodynamic Force Coefficients with Experimental Data

Before examining the physical flow mechanisms underlying the variation of the lift and drag coefficients as presented in Jesson et al. (2015) it is important to verify that the CFD simulation is accurately capturing the flow field by investigating the lift and drag around the model buildings. Comparison is made with results for both buildings at different angles of orientation to the flow direction and for the cube, two building heights above the ground plane. For each experimental configuration (or dataset), ten individual runs were performed and post-processed to provide an ensemble averaged dataset. However, there was significant run to run variation in the experiment results, thus complicating the choice of which run to use when comparing with the simulations. Depending which individual dataset run was used, either good or poor agreement between the simulations and the data could be demonstrated. Likewise, using the ensemble average data is also problematic as the averaging had the effect of smoothing out many of the larger variations within the impinging flow field. Hence can appear as if the experimental results are much smoother than the computational results affecting the comparison with the data. As it is impractical to compare with all runs, it was decided that it was most appropriate to compare with the

ensemble average dataset, to avoid "choosing" the individual run that gave best fit.

Results based on those presented earlier in Haines et al. (2015) are again shown here to illustrate the accuracy of the modelling approach. Figures 6 and 7 illustrate the time varying pressure coefficient on the front face and roof (top) face of the full height cube model at 0° yaw angle. The numerical predictions are compared with the ensemble average experimental results, though the figures also indicate the minimum and maximum values from the experimental runs to illustrate the laboratory variation and the range of measured pressures. This is to address some of the problems of using the ensemble averages as discussed above. The peak pressure on the front face (Figure 6) is reasonably well predicted, as is the transient behaviour once the primary vortex has passed by the cube. Although the magnitude of the fluctuations after the main peak are larger than those shown in the ensemble average experimental results, they are comparable with the range of data measured in the laboratory. Similarly the peak suction on the roof of the cube (Figure 7) is comparable to experiment, though the fluctuations after this peak tend to be larger in magnitude than the experiment. In both cases the main peak is shorter in duration than the experiment, and this is primarily due to the translation speed of the primary vortex being higher in the simulations compared to the experiments. This is most likely due to the different mechanisms for generation of the "downburst" jet in the simulations and the experiments, as discussed in Haines et al. (2015) and Jesson et al. (2015). Figure 8 illustrates the velocity at a radial location of $X/D = 1.5$ on the centre-line of the jet and at a height of $Z/D = 0.03$ above the ground plane. As in the results above, the numerical simulation is compared to the ensemble average of the measure velocity, with the minimum and maximum values from the experiments also shown. Consistent with the pressure results, there is reasonably good agreement between simulations and experiment, with the main discrepancy being the shorter duration of the main peak, again most likely a result of the higher vortex translation speed in the CFD simulations.

Figures 9 to 11 illustrates the aerodynamic force coefficients for the cube building at the 2 heights considered, full height and $40mm$ for 0° yaw angle. Only results for the full height at 45° yaw are presented. In each case, the radial drag coefficient (top left figure), lateral drag coefficient (top right figure) and lift coefficient (lower figure) are presented (using the orientation shown in Figure 5).

On the whole the comparison between predictions and experiment was quite good for all orientations of cube and for all directions. The main issue with the results was identified in the previous section, with the CFD peaks in the drag and lift coefficients being of shorter duration than the laboratory results. Again, the vortex translation speed was higher in the CFD simulation, for the same reasons given earlier arising from differences in the downburst generation mechanism in the simulations and laboratory experiment. However, in most cases, the predicted peak values of the force coefficients agree well with those from the experiments. In the lateral drag results, after the first large peak, which corresponds to the primary vortex passing over the building, the regions

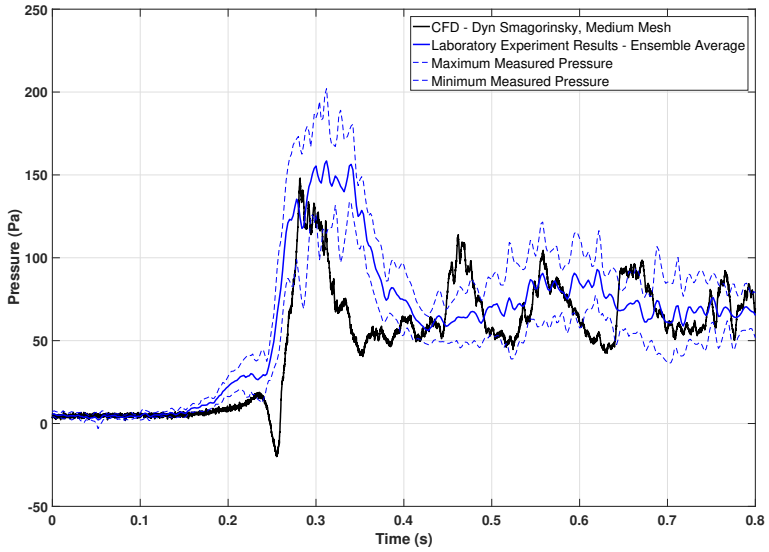

Figure 6: Comparison of Measured and Predicted Pressure in centre of Centre Face of Cube, 0° full height configuration

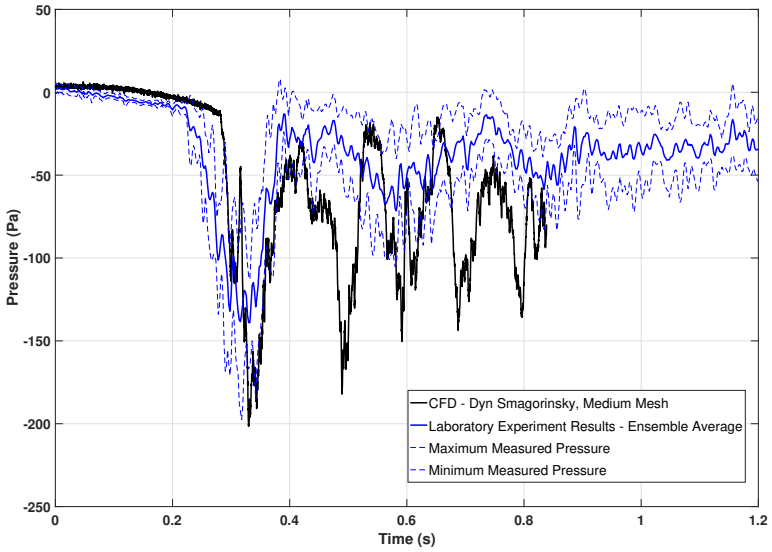

Figure 7: Comparison of Measured and Predicted Pressure in centre of Roof Face of Cube, 0° full height configuration

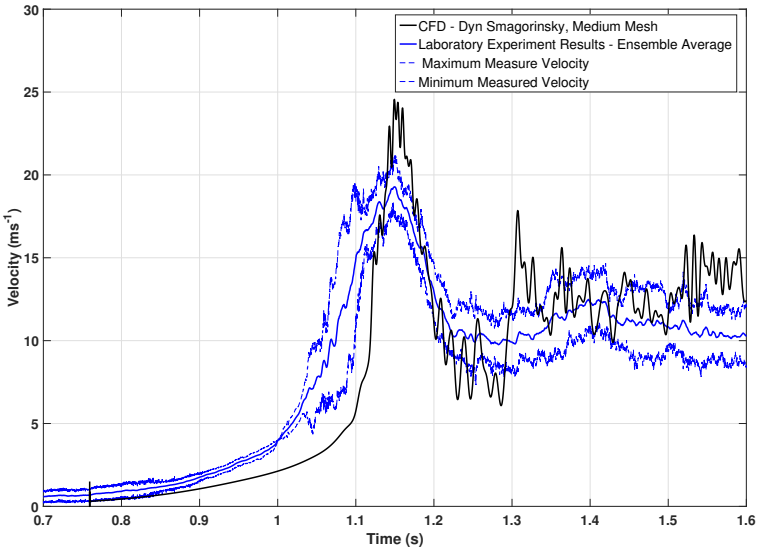

Figure 8: Comparison of Measured and Predicted Velocity at $X/D = 1.5$ on jet centreline at a height of $Z/D = 0.03$ from ground plane.

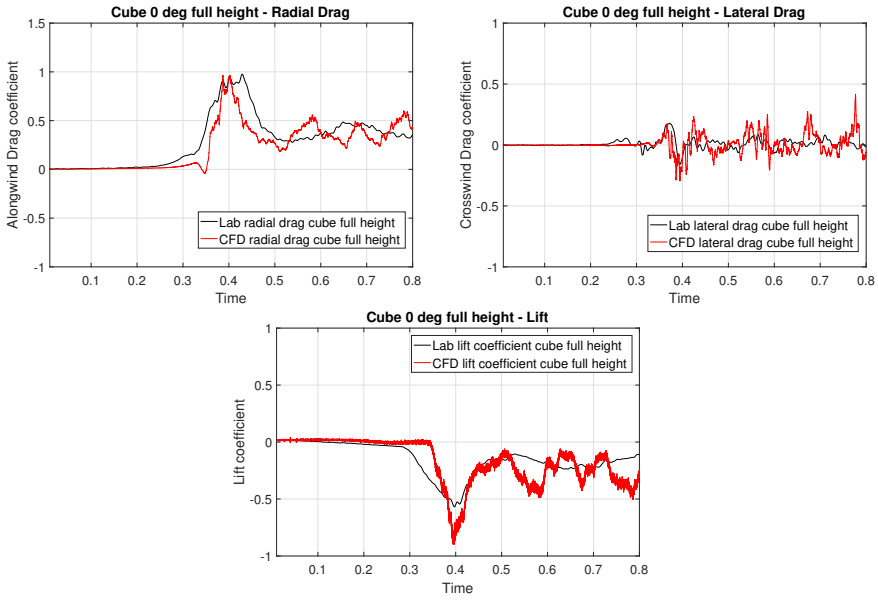

Figure 9: Aerodynamic force coefficients for the cube building at 0° and at full height, compared to data from the laboratory simulations of Jesson et al. (2015).

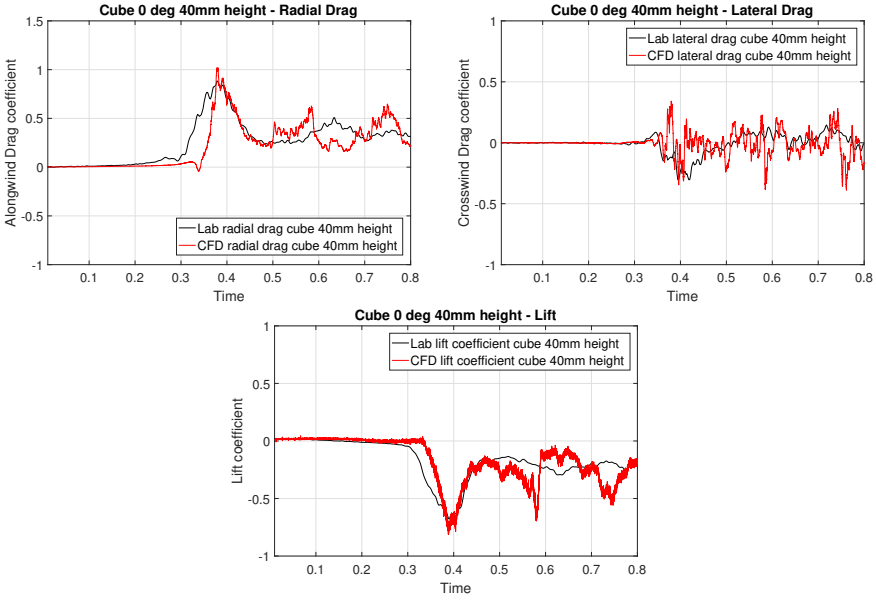

Figure 10: Aerodynamic force coefficients for the cube building at 0° and at 40 mm height, compared to data from the laboratory simulations of Jesson et al. (2015).

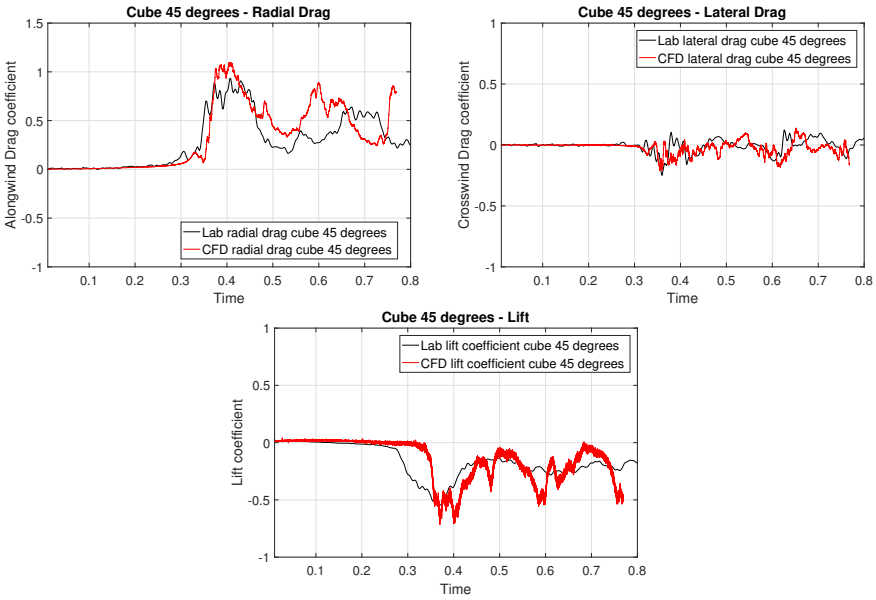

Figure 11: Aerodynamic force coefficients for the cube building at 45° and at full height, compared to data from the laboratory simulations of Jesson et al. (2015).

after this peak matched well to the ensemble average pressure field (unlike the radial drag results). This was caused by the increased run-to-run variation in the experimental results for the lateral drag as a vortex could be shed on the left or right of the building, hence leading to some variations "cancelling" out in the ensemble average. However, for the radial drag the run to run variation would be relatively consistent. The lift coefficients were captured well for all of the building configurations, suggesting that the flow separation is being well captured over the roof of the buildings. The main difference again being the narrower peak in the lift coefficient when compared to the laboratory data due to the faster vortex translation speed. Another issue is noticeable in the simulations when $t \gtrsim 0.7s$, and is due to the difference between the simulation set up and the experimental operation. The jet inlet is set at constant velocity throughout the simulations. However, in the experiment, once the flaps have been released to produce the jet, the fans do not continuously operate and there will be a "drop-off' in velocity as the run continues, a feature that would be complex to model. This is likely to produce discrepancies at later times when comparing the simulations and experimental runs as the inlet velocities will be inconsistent.

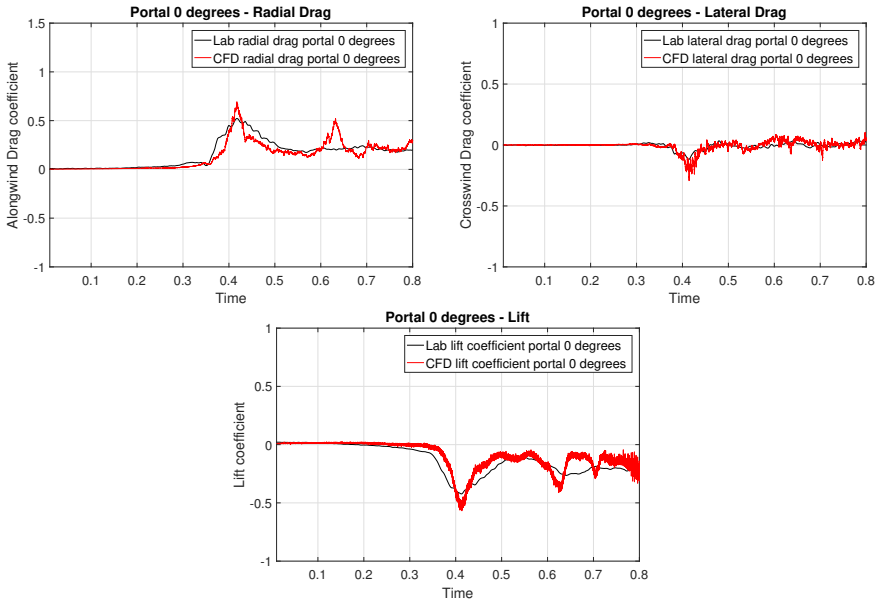

Figure 12: Aerodynamic force coefficients for the portal building at 0° and at full height, compared to data from the laboratory simulations of Jesson et al. (2015).

Similarly, results for the aerodynamic force coefficients on the portal building are illustrated in Figures 12 to 14, for 0°, 45° and 90° yaw, all at full height. In general, the comparison with experimental results is good and particularly for the radial drag and lift, similar characteristics to the results for the cube are demonstrated. Most notably, the peak values are in good agreement though the

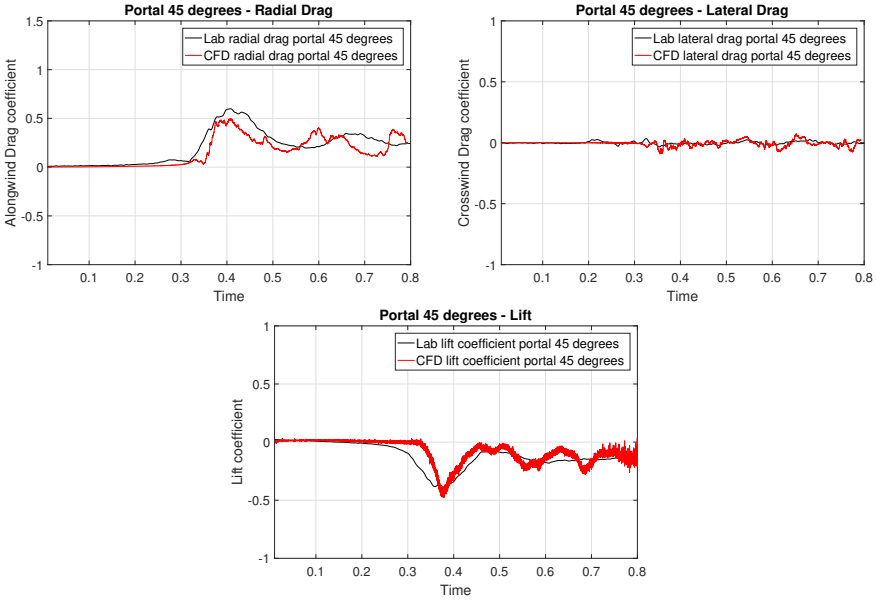

Figure 13: Aerodynamic force coefficients for the portal building at 45° and at full height, compared to data from the laboratory simulations of Jesson et al. (2015).

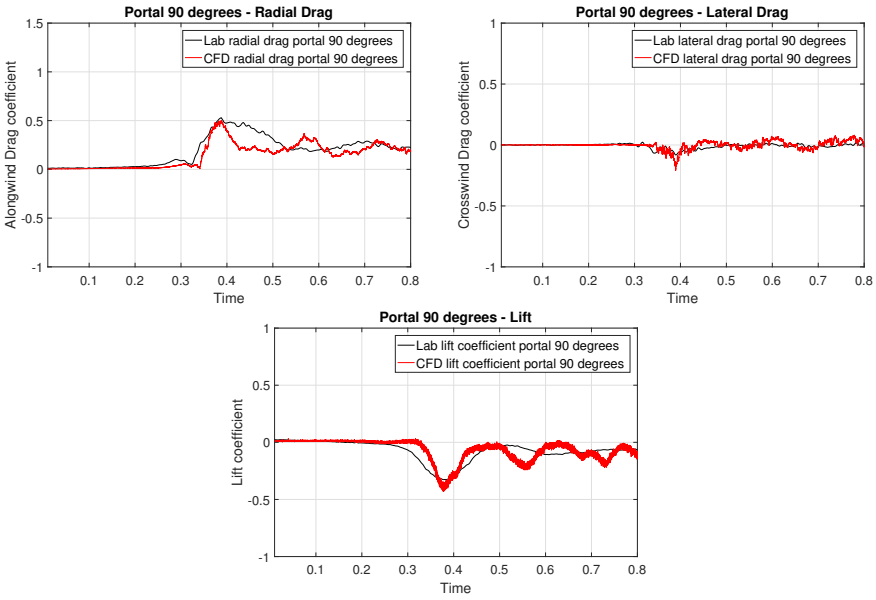

Figure 14: Aerodynamic force coefficients for the portal building at 90° and at full height, compared to data from the laboratory simulations of Jesson et al. (2015).

duration of the peak is less than in the experiment due to the faster translation of the primary vortex. The lateral drag coefficient shows much less variation for the portal building due to the larger aspect ratio of the building and the lower height of the eaves compared to the cube building.

3.2. The Causes of the Drag Around the Buildings

In general, despite the effect of the higher vortex translation speed on the results, the force coefficients for the two building types at various orientations are felt to be sufficiently accurate to be used for further analysis. Jesson et al. (2015) presented a number of conclusions and conjectured flow phenomena in the experimental results for the transient flow field around low rise buildings. Measured pressure distributions on the surfaces of the cube and portal buildings at the time of maximum uplift are shown in Figure 15, reproduced from Jesson et al. (2015). It should be noted that these results and the conjectured flow phenomena highlighted below for the portal building are consistent with similar results presented in Jubayer et al. (2016). The CFD results are now used to visualise the flow field to ascertain the underlying causes of the lift and drag variation along with investigating the questions raised in Jesson et al. (2015). The primary questions raised are summarised below :

1. Vortex Shedding on the Cube.
For the 0° case (and to an extent in the 45° case), at the point of maximum lift, there is a large negative pressure on the sides of the cube, but there is significant difference in the peak values measure (Figure 15i). Additionally, there is an alternating direction in the temporal variation of the lateral force. This imbalance between the pressures on the two sides suggest strong evidence of vortex formation and shedding from the cube occurring alternately on each side. Similar evidence of vortex shedding will be sought in the CFD results to confirm this conjectured conclusion.

2. Conical Vortices on the Cube and Portal Buildings.
For the 45° cube case (image (b) in Figure 15i), there are strong suction pressures on the roof at the windward eaves, with additional evidence of sharp gradients of pressure extending from the leading edges of the roof. There are similar features, though not as clear on the roof of the 45° portal building (image (b) in Figure 15ii). These strong suction pressures are indicative of the strong vorticity due to conical vortices forming at the roof edges, similar to that observed in ABL flows. Flow visualisation in the CFD results will be used to provide confirmation of these flow features.

3. Uplift Differences on Portal Buildings.
Jesson et al. (2015) reports a peak lift coefficient of ~ 0.4 for the 0° portal and of ~ 0.3 for the 90° portal, whereas results from Zhang et al. (2013) suggest that these values will be the same for both the 0° and 90° orientation. However, the differences observed in the uplift between the different yaw angles of the portal building are close to being within the experimental error of $\pm 10\%$ indicated by

Jesson et al. (2015). It is suggested that further studies are required to clarify these differences, and whether there are flow features which contribute to the variation or if it is attributable to experimental error.

4. Pressure Gradients on Portal Building.
The measured pressures on the roof of the cube (0° yaw angle) at the time of maximum lift are nearly constant (image (a) in Figure 15i), with $C_p \approx -0.6$ near the windward edge, dropping to ≈ -0.5 at the leeward edge. Unlike the cube, there are stronger gradients of pressure over the roof of the portal building for both the 0° and 90° yaw angles (images (a) and (c) in Figure 15ii), with windward to leeward variation of C_p of -0.6 to -0.1 on the 0° case and of -0.45 to -0.1 in the 90° case. Other than the roof ridge line in the 0° portal case, the reason for such different variation is not entirely clear from the measured data and warrants further investigation using the CFD analysis.

5. Flow Field Asymmetry Around Buildings.
From the experimental results for the portal building at 0° yaw angle, on the two windward corners of the leading edge of the roof, there are local minima of $C_p = -0.5$ and -0.6, suggesting an asymmetry in the flow. Similarly in the windward half of the roof for the 90° portal building, there are regions of higher suction towards the eaves close to the leading edge, with one side of the roof experiencing a higher value. Whilst this asymmetry is present in the measurements, Jesson et al. (2015) suggests this is exaggerated and is not as evident in animations of the results. The CFD will be investigated to look for evidence of an asymmetry in the downburst flow and pressure results. This feature could be related to that in point 1 above, with vortex shedding occurring on the structure, though this is not as evident in the measured lateral drag coefficients.

3.3. CFD Investigation of Unsteady Flow Phenomena

Pressure coefficients on the roof of the cube and portal buildings are illustrated in Figures 16-20. In each case, the buildings are at the full height and results are presented at a range of yaw angles. In each figure, the images presented are at a time prior to the onset of the primary vortex over the building (top left), just as the primary vortex begins to pass over the structure (top right) and at the point of maximum uplift (bottom). Onset flow is from the left in all cases. In the results for the portal building, the black dotted line indicates the ridge of the roof. These results can be compared directly with the measured data shown in Figure 15 and mostly show good qualitative and quantitative agreement. These results are presented here for clarity and will be used in much of the discussion below on the key points raised from the measurements as highlighted in the previous section.

3.3.1. Vortex Shedding on Cube

Figure 21 shows a plan view of the 0° and 45° cube building respectively, showing the predicted vorticity field at a time of $t = 0.425\,s$ and at $30mm$ height

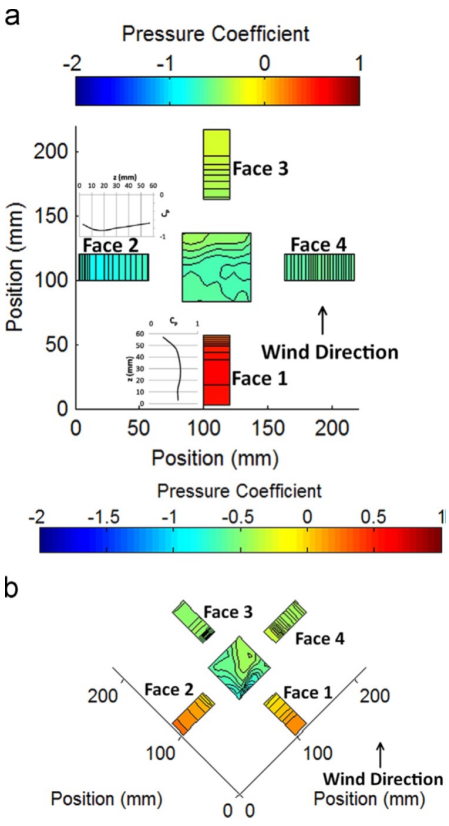

(i) Pressure coefficients at the time of maximum lift over the $60mm$ cube with 0° (a) and 45° (b) yaw angles (Reproduced from Jesson et al. (2015)).

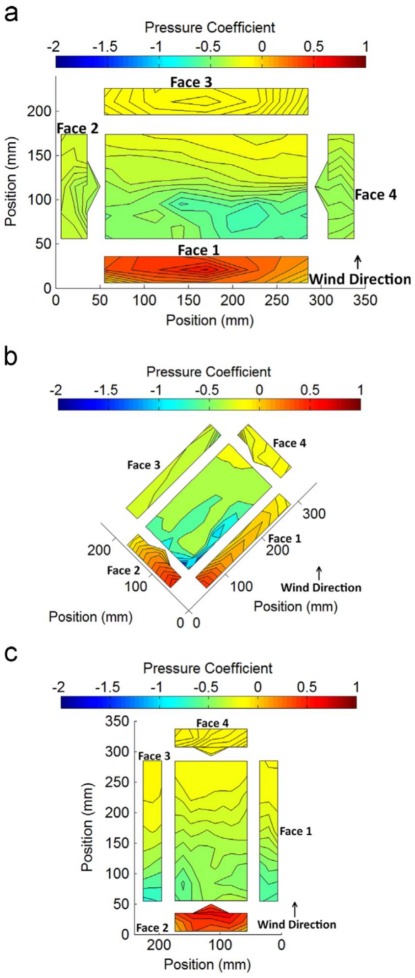

(ii) Pressure coefficients at the time of maximum lift over the portal building at 0° (a), 45° (b) and 90° (c) yaw angles (Reproduced from Jesson et al. (2015)).

Figure 15: Measure pressure coefficients on the cube and portal buildings at time of maximum lift (from Jesson et al. (2015)).

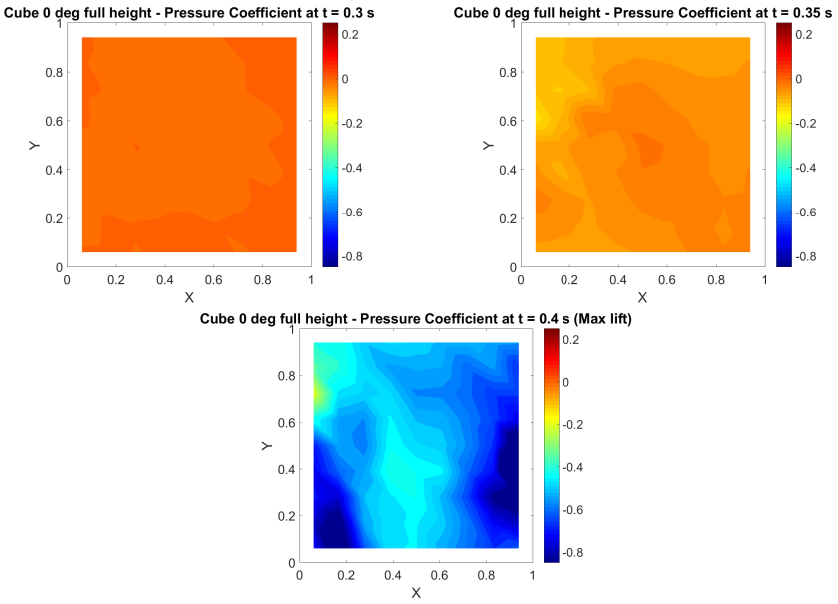

Figure 16: Pressure on roof of cube at 0° yaw angle : results of CFD analysis.

from the ground plane. The vorticity contours (Figure 21) clearly illustrate an asymmetric flow field and in both cases, indicate evidence of different stages of vortex formation on both sides of the cube. That is, vortices shedding from alternate sides of the building, as occurs around buildings in ABL flow for example around the CAARC building (Daniels et al., 2013). From investigation of the wake structure of each case, alternate vortex shedding can also be identified. Figures 22a and 22b compare the predicted lateral drag coefficient for the cube at 0 and 45° yaw angles. Jesson et al. (2015) highlighted that there is an alternating direction in the temporal variation of the lateral force coefficient, and this characteristic is also visible in the CFD results, with a similar frequency and magnitude.

These results illustrate that the flow asymmetry noted in Jesson et al. (2015) for the cube buildings at times close to the maximum lift, are due to vortex shedding from each side of the structure. However, unlike conventional ABL type wind flows, the duration of the phenomenon is short lived and is only present in the downburst flows whilst the primary vortex is passing over the structure. At times later than this, the flow is dominated more by the transient flows due to the downburst.

3.3.2. Conical Vortices on the Cube and Portal Buildings

The measured pressure coefficients close to the windward eaves on the roof of the cube and portal buildings when at 45° yaw angle (Figure 15), indicate

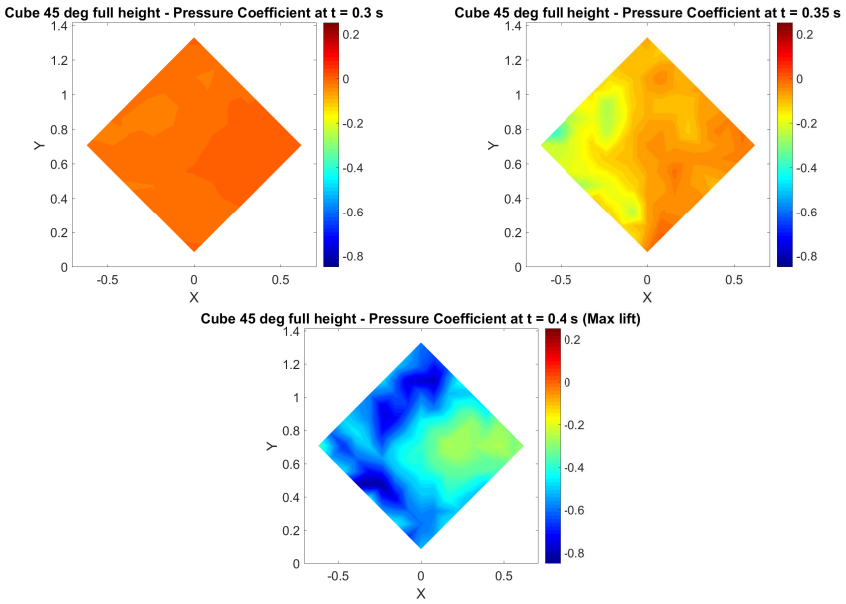

Figure 17: Pressure on roof of cube at 45° yaw angle : results of CFD analysis.

high suction pressures, that have in both cases been interpreted as a "corner vortex". Figures 17 and 19 show the predictions of pressure on the roof of the cube and portal building respectively, at 45° yaw angle as described earlier. Considering the results from the maximum uplift, similar regions of high suction pressures close to the windward eaves are clear, and the pressure distribution is qualitatively in good agreement with those presented in Jesson et al. (2015). Additionally, the initial development of the corner vortices can be seen close to the windward corner of the structures, just as the primary vortex interacts with the buildings.

Figure 23 illustrates iso-surfaces of vorticity for the portal building at the point of maximum lift, with the surfaces coloured using the velocity magnitude. The flow structure highlights that conical vortices are forming on the leeward edge of roof of the building and thus confirm that the suction pressures close to the windward eaves on the roof of the portal building at the 45° yaw angle were caused by conical vortices. This also matches with the findings of Jubayer et al. (2016) and Zhang et al. (2013) who also observed conical vortices being formed on the leading edge in their flow visualisation study of a laboratory based impinging jet.

For the cube at the 45° yaw angle, initially the suctions on the roof are driven by the separation bubble formed as the primary vortex interacted with the windward edge of the roof. At this time ($0.375s$) the greatest lift coefficient was recorded (Figure 11). However, these lift results also showed a secondary

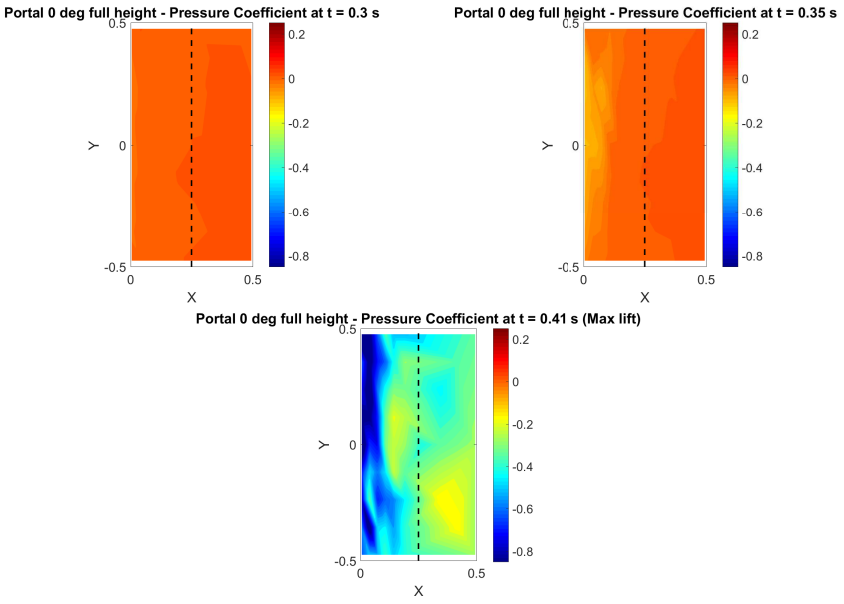

Figure 18: Pressure on roof of portal building at 0° yaw angle : results of CFD analysis.

peak at $0.42s$, not present in the ensemble average of Jesson et al. (2015). This corresponded to the conical vortices forming on the roof of the cube at $0.4s$ illustrated in Figure 24. These conical vortices would give rise to a pressure gradient across the roof but were not observed by Jesson et al. (2015) as the pressure gradients on the roof at the 45° yaw angle were : 1) only examined at the time of maximum lift and 2) plotted for the ensemble average, where there is no secondary peak.

The secondary peak is likely not present in the ensemble of Jesson et al. (2015) because slight differences in the translational velocities of the primary vortex would give rise to different timings of the conical vortices forming. This helps to explain why the secondary peaks are not present in the ensemble average in Figure 11 and also why the peak lift is so wide compared to the other peak lift coefficients for the cube which are illustrated in Figures 9-10.

3.3.3. Uplift Differences on Portal Buildings

Figures 13 and 14 illustrate that the 45° and 90° yaw angle lift coefficients for the portal building were similar at ≈ -0.4 and that any differences observed between these two yaw angles were likely to be caused by experimental variation. However, the 0° yaw angle portal building, illustrated in Figure 12 had a higher magnitude lift coefficient of ≈ -0.55, which is also notably different to the laboratory results. However, this discrepancy could again be attributed to the higher predicted vortex translation velocity as described earlier. Although

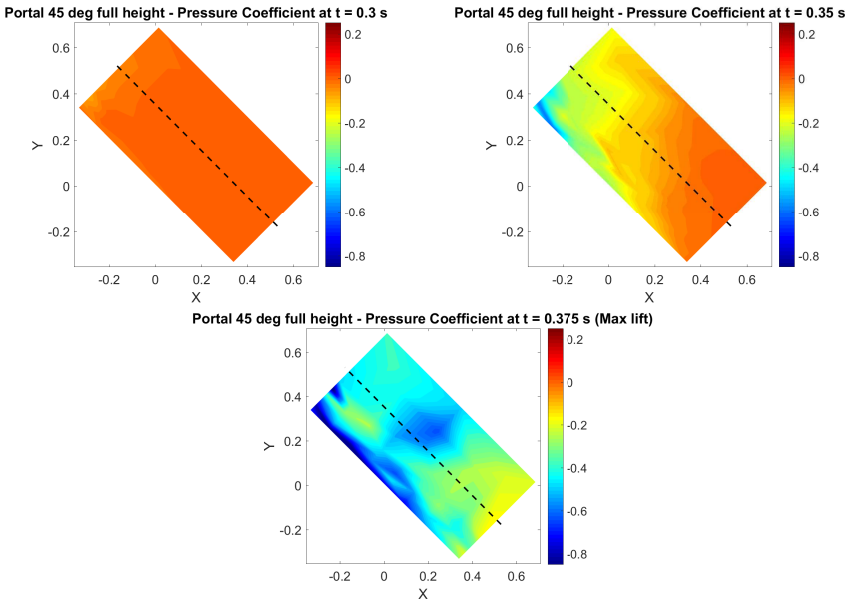

Figure 19: Pressure on roof of portal building at 45° yaw angle : results of CFD analysis.

Figure 7 shows results for the centre of the roof of the cube, using these results as a guide, the peak lift is higher in magnitude than experiment and the peak width is narrower due to the higher vortex translation speed. It is likely that the portal building results have similar characteristics, hence, the lift at 0° angle is likely to be increased.

The pressure coefficient on the roof of the portal buildings at 0° yaw angle are illustrated in Figures 18, and at the point of maximum lift, a large suction is on the roof just down stream of the windward edge of the roof, characteristic of flow separation downstream of the windward eaves. As this separation at the windward eaves dominates the flow structure over the roof of the building, the stronger suction due to the higher vortex translation speed will cause the higher lift on the roof. In the 45° case, the corner vortex has most influence but over less of the roof surface (Figure 19), and for the 90° case, the narrower building width perpendicular to the onset flow mean any separated flow will act over a narrower area (Figure 20). Hence the uplift is similar in those two cases and is not as strongly affected by the vortex translation speed.

These results tend to confirm that the peak uplift on the portal building is largely constant with varying yaw angle, and any differences in the measured data are most likely due to experimental variation.

3.3.4. Pressure Gradients on Portal Building

Jesson et al. (2015) was unable to explain why there were strong gradients

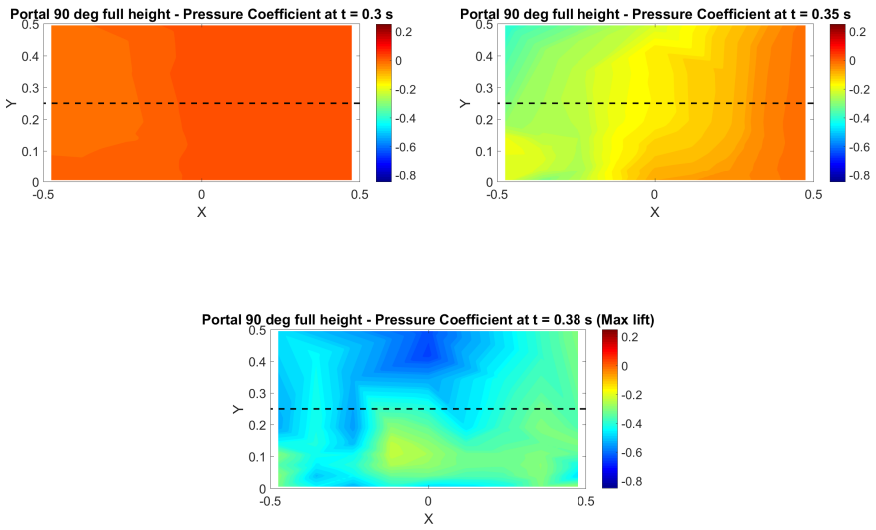

Figure 20: Pressure on roof of portal building at 90° yaw angle : results of CFD analysis.

of pressure which formed over the portal building but not the cube. However as mentioned above in section 3.3.3, the strong gradients of pressure on the portal building at 0° and 90° were mainly due to flow separation on the roof at the windward eaves. Compared to the experimental data (Figure 15ii), the predicted separation region (Figures 18 and 20) extends over a larger region downstream of the front edge of the building, and as with previous conclusions, this is most likely due to the higher vortex translation speed.

For the cube at 0°, there is much less variation in pressure coefficient on the roof than the portal building (Figure 15i), though this is not the case in the CFD results (Figure 16). Another difference noted between the cube and portal building is that the lift coefficients, and also suction pressures, were generally higher for the cube building, which Jesson et al. (2015) attributed to the less streamlined cube building giving rise to greater flow separation, hence greater suction and lift coefficients on the roof. Whilst there is flow separation at the roof windward edge of the cube, the iso-vorticity plots for the cube at 0° (Figure 25), illustrate that the flow around and over the cube at this orientation is dominated by vortex shedding as the primary vortex passes over the building. The plan view of the cube just after the time of maximum lift (Figure 21a) also demonstrates the vortex shedding present in the flow. Additionally, these figures indicate an asymmetry to the flow field arising from the vortex shedding as discussed in section 3.3.1, which corresponds to the asymmetric pressure coefficient distribution on the cube roof at the time of maximum lift (Figure

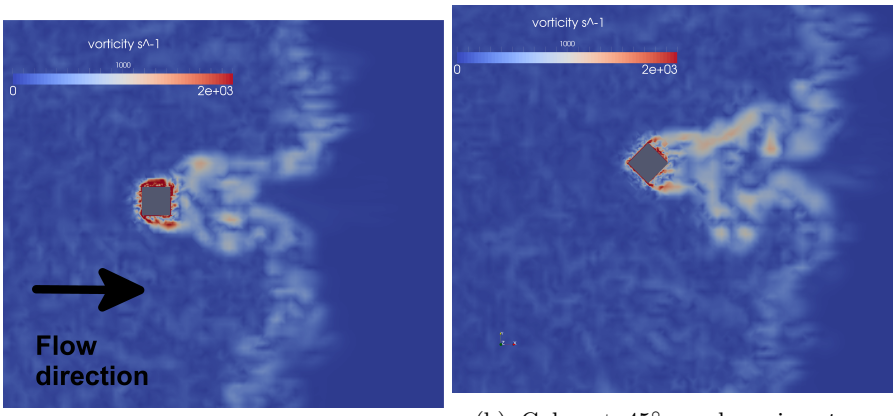

(a) Cube at 0° : plan view $t = 0.425s$.

(b) Cube at 45° : plan view $t = 0.425s$.

Figure 21: The vorticity contours at a height of $30mm$ illustrating the vortex shedding on the sides of the cube building at the 0° and 45° yaw angles.

16).

For the 45° yaw cases, the flow over the roof is dominated by the corner vortices as discussed in section 3.3.2 with no further discussion required here.

3.3.5. Flow Field Asymmetry Around Buildings

The slight flow field asymmetry around the portal buildings observed by Jesson et al. (2015) was likely caused by a slight misalignment in the yaw angle of the building in the laboratory simulator, as hypothesised. There was no bias to the side to which vortex shedding occurred in the CFD simulations. They shed from one side then the other (as they would in ABL flows) and showed no bias as to which side the vortex was initially shed from. This is illustrated well in Figures 26 and 27, which illustrates the vortex shedding around the portal building at the 0° and 90° yaw angles.

From these figures it is also possible to see that the flow separation and vortex shedding is reduced compared to the cube, as illustrated in Figure 21, mainly due to the lower height of the portal building compared to the cube. This also explains why the lateral drag was reduced for the portal building at all yaw angles compared to the cube (Figures 9 and 12-14).

3.4. Comparison to Existing ABL Codes

Jesson et al. (2015) considered the implications for building codes given the potential for differences from ABL flow from downburst / impinging jets. Similarly the CFD flow visualisation from the simulated downburst flows is also used to assess any differences in flow phenomena with those usually expected in an ABL flow field around a building.

Figures 21, 26 and 27 illustrate that flow separation and vortex shedding does still occur around a building in downburst like flow. However, while the

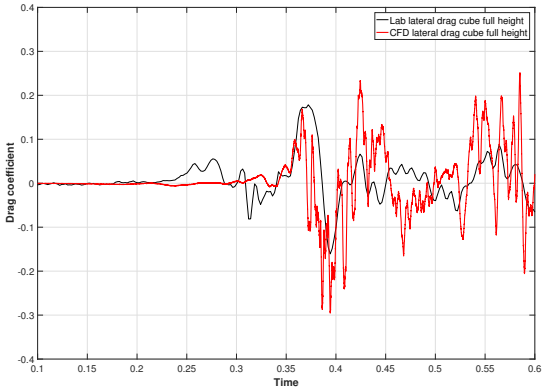

(a) Cube at 0° Lateral Drag Coefficient.

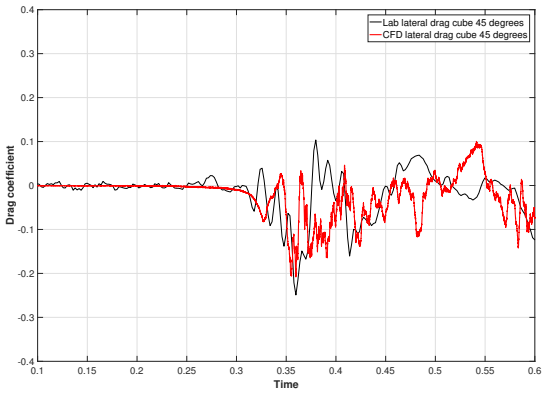

(b) Cube at 45° Lateral Drag Coefficient.

Figure 22: Lateral Drag Coefficient for the Cube Building - Comparison between CFD results and Laboratory Experiments.

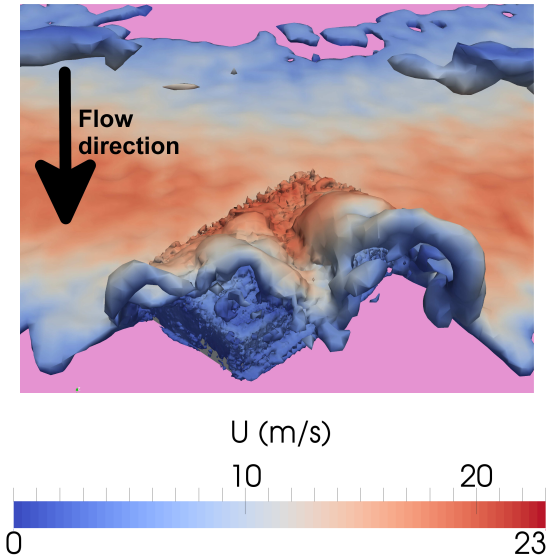

Figure 23: The $550s^{-1}$ vorticity iso-surface coloured by velocity on the portal building at 45° yaw angle : view from rear at point of maximum lift, $t = 0.375s$.

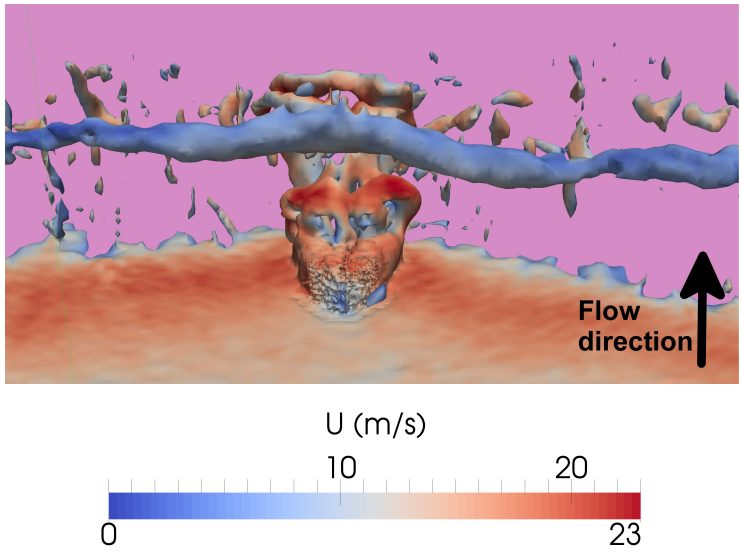

Figure 24: The $550s^{-1}$ vorticity iso-surface around the cube building at the 45° yaw angle - view from front at time $t = 0.4s$.

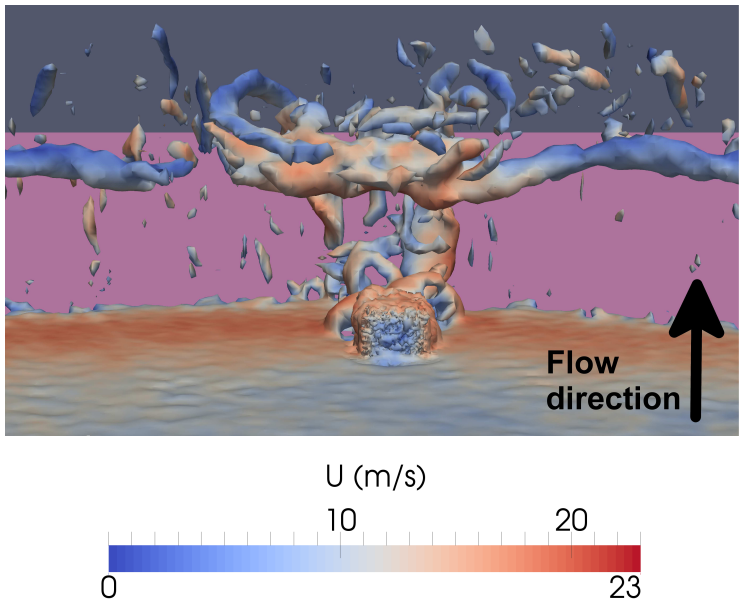

Figure 25: The $550s^{-1}$ vorticity iso-surface around the cube building at the 0° yaw angle - view from front at $t = 0.425s$.

primary vortex of a downburst might exceed ABL wind loading (Jesson et al., 2015) the secondary and rear vortices formed during a downburst are weaker resulting in a reduction in vortex shedding with time. Additionally, the onset flow arising due to the primary vortex translation is much shorter in duration than the less transient wind speed in ABL flows. This would make it difficult for effects such as building resonance in tall buildings to be established during a downburst and this is made even more unlikely when the short duration of a downburst is considered.

Whilst downburst flows are less likely to cause structural problems due to vortex-induced vibrations, there are other more significant effects to consider. The sudden change in pressure due to downbursts increases the chance of cladding or window damage and the pressure gradient observed across the roof of the portal building could potentially lead to the removal of tiles along the roof region which the conical vortex influences (illustrated on the portal building at 45° in Figure 23). Although, it is acknowledged that the conical vortex formed from roof edges is not exclusive to the downburst and they have been observed in ABL flows (Wu, 2001).

There was also evidence of a horizontally aligned rear vortex appearing on the leeward face of the building, illustrated for the cube at the 0° yaw angle in Figure 28. This flow feature has also been observed to occur as a transient feature in ABL flows (Arya, 1988; Kareem, 2012). Figure 28 also showed that the presence of a building caused the primary vortex to "jump" over the building,

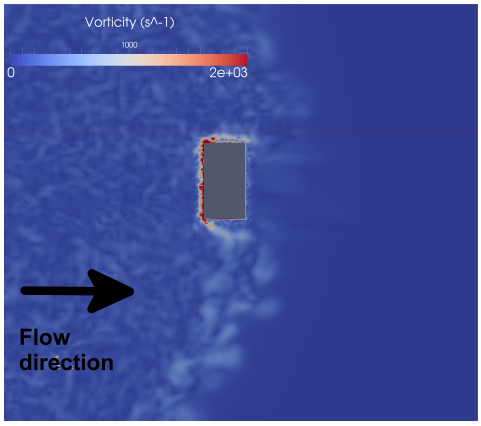

(a) Portal Building at 0° - time $t = 0.4s$.

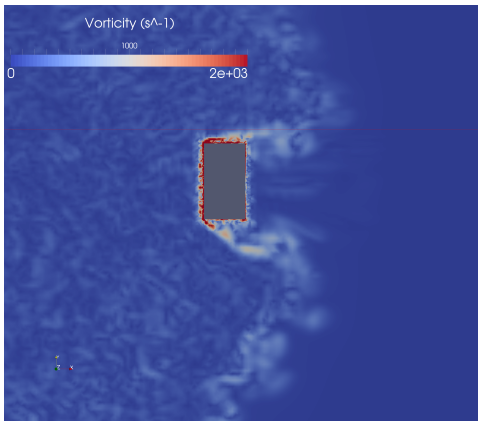

(b) Portal Building at 0° - time $t = 0.425s$.

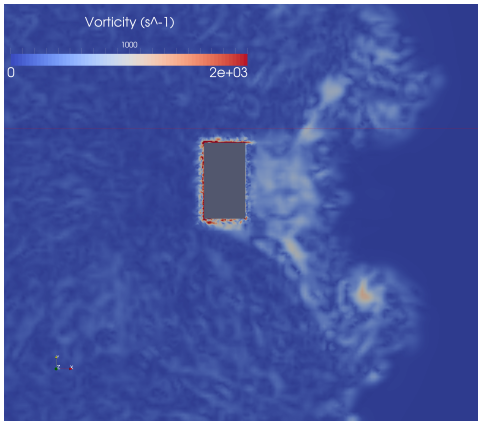

(c) Portal Building at 0° - time $t = 0.475s$.

Figure 26: Contours of vorticity at a $30mm$ height for the portal building at the 0° yaw angle.

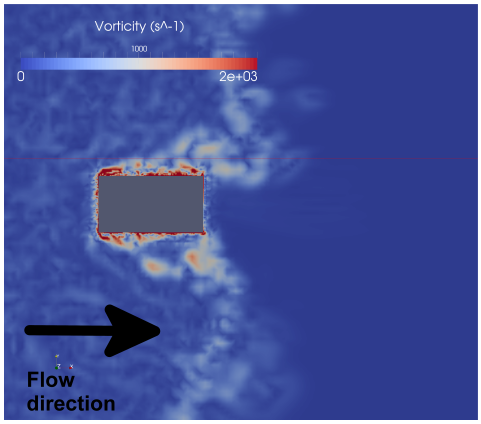

(a) Portal Building at 90° - time $t = 0.4s$.

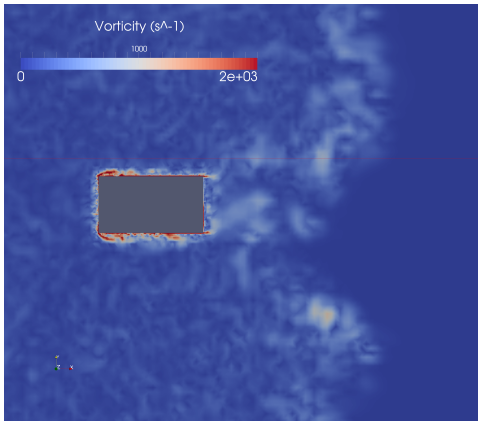

(b) Portal Building at 90° - time $t = 0.45s$.

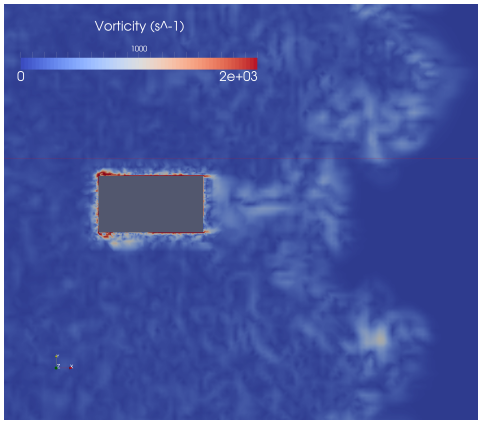

(c) Portal Building at 90° - time $t = 0.475s$.

Figure 27: Contours of vorticity at a $30mm$ height for the portal building at the 90° yaw angle.

maintaining its vortex like structure but with the vortex core gaining height compared with the vortex when unimpeded. This is also illustrated in Figure 29, with the flow on the left side of the figure not influenced by any building and the flow on the right side affected due to the presence of the cube building. The effect of the building on causing a vortex "jump" is clear. This effect could potentially lead to interference type effects for buildings in the wake of the first building.

From the above it would appear that the majority of flow features which occur for downburst flows are also present as transient phenomena in ABL flows. The only exception to this is the size of the vortices which form from the roof of the building. The primary vortex is lifted up by the presence of a building and gains height when compared to there being no building presence. As there is no horizontally aligned vortex in the ABL flow field this phenomena is not observed.

4. Conclusion

This paper presented results from a CFD simulation of the laboratory based impinging jet simulator of Jesson et al. (2015). The CFD simulation was found to be able to reproduce the drag and lift coefficients found from the laboratory simulation accurately.

The CFD simulation was then used to visualise the flow field around the buildings investigated in Jesson et al. (2015) and find the causes of some unexplained pressure and drag coefficient results. Firstly the CFD confirmed that vortex shedding was indeed occurring as predicted from the lateral and lift experimental data.

The presence of conical vortices at certain yaw angles of the portal building was also confirmed. This led to a sharp gradient of pressure across the roof of the portal building as well as being the cause of differences in lift coefficient between the 0° and 45° and 90° yaw angles of the portal building, which Jesson et al. (2015) had previously attributed to experimental variation. The conical vortices on the portal building also led to an increase in lift on the portal buildings when compared with the cube at the 0° yaw angle, which was driven only by the flow separating at the roof leading edge.

No evidence was found of the flow asymmetries observed around the sides of the portal building. The cause of these flow asymmetries was likely due to a slight building alignment rather than a phenomenon specific to downburst flow.

In addition to confirming the hypotheses of Jesson et al. (2015) the investigation also found evidence of other flow phenomenon including small vortices forming on the rear face of the buildings at the 0° and 90° yaw angles. The primary vortex was also found to "jump" over the low rise buildings, maintaining its vortex like structure but with the vortex core at a greater height than when there was no building present.

The cause of the greater lift coefficients on the cube at the 45° yaw angle over the cube at the 0° yaw angle was also found. Conical vortices formed on the

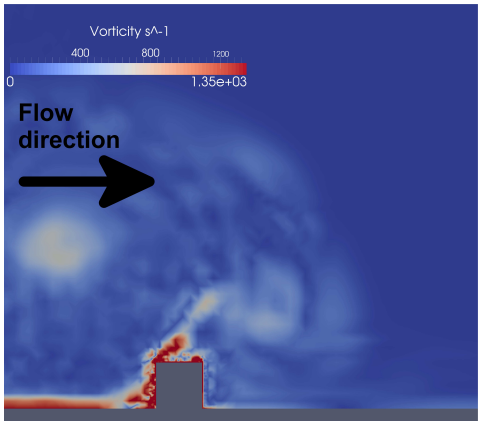

(a) Cube Building at 0° - time $t = 0.375s$.

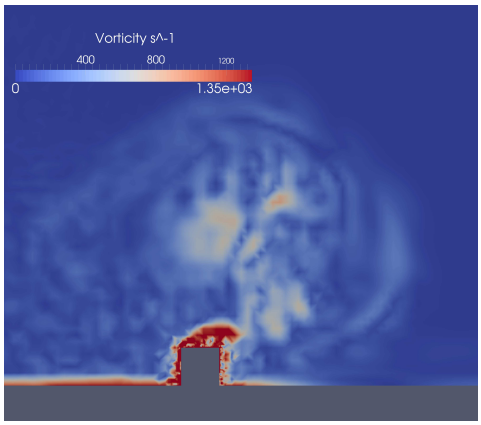

(b) Cube Building at 0° - time $t = 0.4s$.

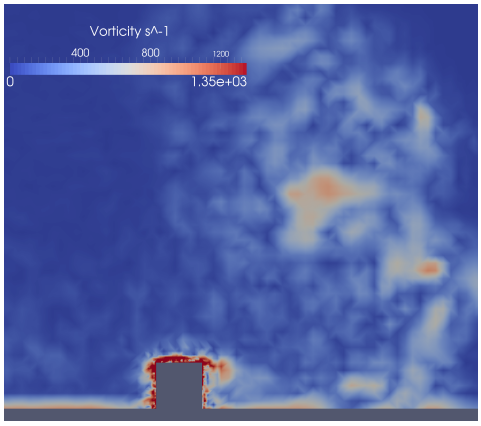

(c) Cube Building at 0° - time $t = 0.425s$.

Figure 28: The presence of vorticity on the rear face of the cube building at the 0° yaw angle.

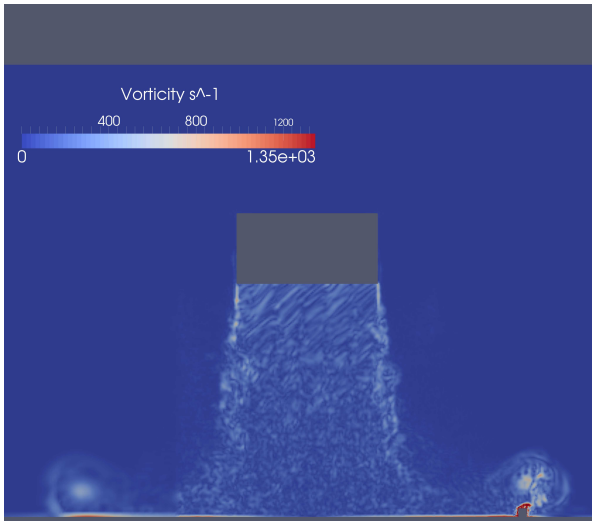

(a) Time $t = 0.4s$.

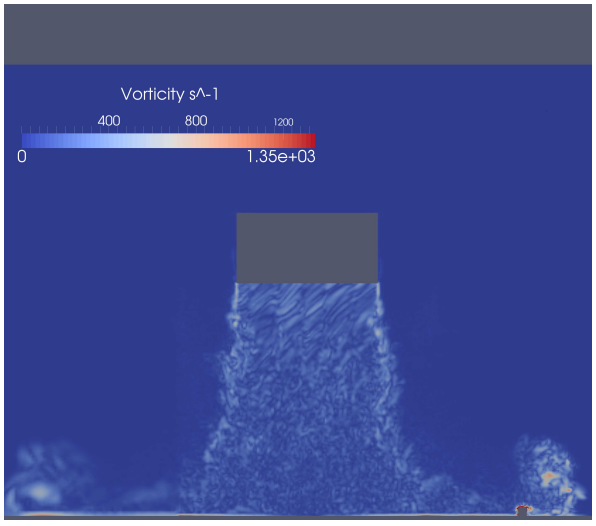

(b) Time $t = 0.425s$.

Figure 29: The influence of the building on the location of the vortex core of the primary vortex.

windward edges of the roof at the 45° yaw angle after the initial flow separation caused by the primary vortex. This led to a double peak in the maximum lift coefficient which was not observed by Jesson et al. (2015) as they were averaged out.

The work has also highlighted a number of flow phenomenon which would be of interest to study in further research. Specifically the potential effect the vortex "jumping" over a low rise building might have on buildings in the leeward region, the impact of the conical vortices forming in relation to cladding damage and also the impact of the sudden pressure change on cladding.

5. Acknowledgements

The authors would like to express their gratitude to the EPSRC for their support for this research through grant EP/J008370/1. Additionally, the authors would like to acknowledge the support and collaboration of Prof Mark Sterling and Dr Mike Jesson, Department of Civil Engineering, University of Birmingham, Birmingham, UK, for the experimental data provided from the impinging jet simulator and for their contribution to the discussion and understanding of the results.

The data presented within the paper may be accessed from the digital record http://dx.doi.org/10.5525/gla.researchdata.490.

References

Arya, S., 1988: *Introduction to micrometeorology*. Academic press inc., 307 pp.

ASCE, 2006: Minimum design loads for buildings and other structures. *ASCE/SEI 7-05*, Reston, VA, ASCE.

ASCE, 2010: Minimum design loads for buildings and other structures. *ASCE/SEI 7-05*, Reston, VA, ASCE.

Castro, I. and A. Robins, 1977: The flow around a surface mounted cube in uniform and turbulent streams. *Journal of fluid mechanics*, **79(2)**, 307–335.

Chay, M. and C. Letchford, 2002a: Pressure distributions on a cube in a simulated thunderstorm downburst, part a: stationary downburst observations. *Journal of wind engineering and industrial Aerodynamics*, **90**, 711–732.

Chay, M. and C. Letchford, 2002b: Pressure distributions on a cube in a simulated thunderstorm downburst, part b: moving downburst observations. *Journal of wind engineering and industrial aerodynamics*, **90**, 733–753.

Daniels, S., I. Castro, and Z.-T. Xie, 2013: Peak loading and surface pressures fluctuations of a tall building. *Journal of wind engineering and industrial aerodynamics*, **120**, 19–28.

Fujita, T., 1985: Downburst: Microburst and macroburst. *University of Chicago Press, IL*, pp. 122.

Haines, M., I. Taylor, M. Jesson, and M. Sterling, 2015: The numerical simulation of a pulsed impinging jet using modern turbulence models. *Proceedings of the 14th international conference on wind engineering*, Porto Alegre, Brazil, ICWE, ID 1869.

Holmes, J., 1992: Physical modelling of thunderstorm downdrafts by wind tunnel jet. *Second AWES workshop*, Monash University, USA, AWES, 29–32.

Jesson, M., M. Sterling, C. Letchford, and M. Haines, 2015: Aerodynamic forces on generic buildings subject to transient, downburst-type winds. *Journal of wind engineering and industrial aerodynamics*, **137**, 58–68.

Jubayer, C., A. Elatar, and H. Hangan, 2016: Pressure distributions on a low-rise building in a laboratory simulated downburst. *Proceedings of the 8th International Colloquium on Bluff Body Aerodynamics and Applications*, Boston, Massachusetts, USA, June 2016.

Kareem, A., 2012: Modelling of transient winds and their load effects on structures. *Proceedings of the 10th UK conference on wind engineering*, Southampton, UK, WES, 3–21.

Kim, J. and H. Hangan, 2007: Numerical characterization of impinging jets with application to downbursts. *Journal of wind engineering and industrial aerodynamics*, **95**, 279–298.

Kim, Y., I. Castro, and Z.-T. Xie, 2013: Divergence free turbulence inflow conditions for large eddy simulations with incompressible flow solvers. *Computers and fluids*, **84**, 56–68.

Kornev, N. and E. Hassel, 2007: Method of random spots for generation of synthetic inhomogeneous turbulent fields with prescribed autocorrelation functions. *Communications in numerical methods in engineering*, **23**, 35–43.

Lin, W., 2010: Validation of a novel downdraft outflow simulator, a slot jet wind tunnel. Ph.D. thesis, University of Western Ontario.

Lin, W. and E. Savory, 2006: Large-scale quasi steady modelling of a downburst outflow using a slot jet. *Wind and structures*, **9**, 419–440.

Lombardo, F., 2009: Analysis and interpretation of thunderstorm wind flow and its effects on a bluff body. Ph.D. thesis, Texas Technical University, [PhD thesis available from Atmospheric Science group, Texas Technical University].

Poletto, R., T. Craft, and A. Revell, 2013: A new divergence free synthetic eddy method for the reproduction of inlet flow conditions for les. *Flow turbulence and combustion*, **91**, 519–539.

Selvam, R. and J. Holmes, 1992: Numerical simulation of thunderstorm downdrafts. *Journal of wind engineering and industrial aerodynamics*, **44(4)**, 2817–2825.

Sengupta, A. and P. Sarkar, 2008: Experimental measurement and numerical simulation of an impinging jet with application to thunderstorm microburst winds. *Journal of wind engineering and industrial aerodynamics*, **96(3)**, 345–365.

Sterling, M., C. Baker, M. Haines, and A. Quinn, 2011: Scaling a thunderstorm downburst simulator. *13th International Conference on Wind Engineering*, RAI, Amsterdam, The Netherlands, ICWE.

Sterling, M., C. Baker, P. Richards, R. Hoxey, and A. Quinn, 2006: An investigation of the wind statistics and extreme gust events at a rural site. *Wind and structures*, **9(3)**, 193–216.

Wu, F., 2001: Full-scale study of conical vortices and their effects on roof corners,. Ph.D. thesis, Texas Tech University, 198 pp.

Xu, Z. and H. Hangan, 2008: Scale, boundary and inlet condition effects on impinging jets. *Journal of wind engineering and industrial dynamics*, **96**, 2383–2402.

Zhang, Y., P. Sarkar, and H. Hu, 2013: An experimental study of flow fields and wind loads on gable roof building models in microburst like wind. *Experiments in fluids*, **54:1511**, 1–21.